AGU PUBLICATIONS

Geophysical Research Letters

RESEARCH LETTER
10.1002/2017GL072841

Special Section:
Early Results: Juno at Jupiter

Key Points:
- Hot spots are confirmed as very dry regions in the atmosphere of Jupiter
- Consistent spatial patterns are found in the distributions of water and phosphine
- Ammonia shows local enhancements in the southern parts of hot spots

Supporting Information:
- Text S1

Correspondence to:
D. Grassi,
davide.grassi@iaps.inaf.it

Citation:
Grassi, D., et al. (2017), Preliminary results on the composition of Jupiter's troposphere in hot spot regions from the JIRAM/Juno instrument, *Geophys. Res. Lett.*, *44*, doi:10.1002/2017GL072841.

Received 27 JAN 2017
Accepted 21 MAR 2017

Preliminary results on the composition of Jupiter's troposphere in hot spot regions from the JIRAM/Juno instrument

D. Grassi[1], A. Adriani[1], A. Mura[1], B. M. Dinelli[1,2], G. Sindoni[1], D. Turrini[1,3], G. Filacchione[1], A. Migliorini[1], M. L. Moriconi[1,4], F. Tosi[1], R. Noschese[1], A. Cicchetti[1], F. Altieri[1], F. Fabiano[2,5], G. Piccioni[1], S. Stefani[1], S. Atreya[6], J. Lunine[7], G. Orton[8], A. Ingersoll[9], S. Bolton[10], S. Levin[8], J. Connerney[11], A. Olivieri[12], and M. Amoroso[12]

[1]Istituto di Astrofisica e Planetologia Spaziali, INAF, Rome, Italy, [2]Istituto di Scienze dell'Atmosfera e del Clima, CNR, Bologna, Italy, [3]Departamento de Fisica, Universidad de Atacama, Copiapò, Chile, [4]Istituto di Scienze dell'Atmosfera e del Clima, CNR, Rome, Italy, [5]Dipartimento di Fisica e Astronomia, Università di Bologna, Bologna, Italy, [6]Department of Climate and Space Sciences and Engineering, University of Michigan, Ann Arbor, Michigan, USA, [7]Cornell Center for Astrophysics and Planetary Science, Cornell University, Ithaca, New York, USA, [8]Jet Propulsion Laboratory, California Institute of Technology, Pasadena, California, USA, [9]California Institute of Technology, Pasadena, California, USA, [10]Southwest Research Institute, San Antonio, Texas, USA, [11]NASA Goddard Space Flight Center, Greenbelt, Maryland, USA, [12]Agenzia Spaziale Italiana, Matera, Italy

Abstract The Jupiter InfraRed Auroral Mapper (JIRAM) instrument on board the Juno spacecraft performed observations of two bright Jupiter hot spots around the time of the first Juno pericenter passage on 27 August 2016. The spectra acquired in the 4–5 μm spectral range were analyzed to infer the residual opacities of the uppermost cloud deck as well as the mean mixing ratios of water, ammonia, and phosphine at the approximate level of few bars. Our results support the current view of hot spots as regions of prevailing descending vertical motions in the atmosphere but extend this view suggesting that upwelling may occur at the southern boundaries of these structures. Comparison with the global ammonia abundance measured by Juno Microwave Radiometer suggests also that hot spots may represent sites of local enrichment of this gas. JIRAM also identifies similar spatial patterns in water and phosphine contents in the two hot spots.

1. Introduction

Most of the information currently available on the composition of Jupiter's troposphere derives from remote-sensing data. Among these data sets, a special role has been played by infrared spectroscopy.

While most of the spectrum between 0.4 and 4 μm is dominated by the strong absorption features of methane, a spectrally transparent region exists around 5 μm. This region lies far enough from the peak of the solar emission toward the infrared to be largely dominated by the thermal emission of the atmosphere. It hosts the spectral lines of several trace constituents of Jupiter's atmosphere. Among them are H_2O and NH_3, which are the main carriers of oxygen and nitrogen in the Jupiter's envelope, respectively.

Jupiter's emission at 5 μm has been measured in the past at low latitude and midlatitude from space [*Carlson et al.*, 1993; *Roos-Serote et al.*, 1999; *Giles et al.*, 2015] and ground-based observations [e.g., *Fletcher et al.*, 2016; *Giles et al.*, 2016]. At these wavelengths, the Jupiter disk presents strong signal contrasts, exceeding a factor 100 in radiance.

Most areas appear dark (brightness temperatures below 200 K), implying relatively low temperatures of the emitting layers and suggesting a global cover of optically thick clouds. In fact, globally averaged thermochemical equilibrium models predict three separate cloud layers composed of ammonia ice, ammonium hydrosulfide ice, and water ice/liquid, extending over several tens of kilometers in altitude [*Atreya et al.*, 1999]. The brightness temperature study by *Drossart et al.* [1998] demonstrated that at least in the equatorial region the uppermost cloud of NH_3 ice must have residual transparency, allowing some radiation from the warmer regions below to escape to space. Further analysis [*Irwin et al.*, 2001] found that changes in brightness at 5 μm are correlated not with variability of the higher ammonia cloud, but rather with opacity variations associated with cloud layers between 1 and 2 bar pressure, perhaps ammonium hydrosulfide.

However, some regions show much higher signals (brightness temperatures above 260 K), which implies that the thermal photons emitted at an effective level of few bars are marginally absorbed by the clouds (i.e.: optical depth < 1), providing an effective probe of the deeper (and warmer) part of the troposphere. The ultimate source of opacity at 5 μm is molecular hydrogen collision-induced absorption, which, even in the absence of other minor constituents or clouds, reaches an optical thickness of 1 around the 5.5 bar level.

Among the bright areas, the so-called "hot spots' stand out as the most intense features. Hot spots are associated with the grey "festoons" or blush "dark projections" observed in the optical domain between the equatorial zone and the north equatorial belt. *Rogers* [1995] provided a review of historical observation of these structures. While their dynamical properties are an active area of investigation [*Arregi et al.*, 2006; *Showman and Dowling*, 2000], the hot spots are long known to be regions of low cloud opacity [*Terrile and Westphal*, 1977; *Ortiz et al.*, 1998]. Spectra of hot spots in the 5 μm region have been investigated in detail by a number of researchers [*Irwin et al.*, 1998; *Roos-Serote et al.*, 1998; *Nixon et al.*, 2001], who analyzed data mainly from the Galileo Near-Infrared Mapping Spectrometer (NIMS).

Volatile abundances and structure in a single hot spot were measured in situ by the Galileo Entry Probe (GEP) during its descent in Jupiter's atmosphere on 7 December 1995. The probe entered at 6.5°N, −4.9°E, at the southern rim of a hot spot [*Orton et al.*, 1998]. While these data provide an easily interpretable set of abundances in the case of the noble gases and noncondensables such as CH_4 [*Niemann et al.*, 1998] it is still unclear to what extent the abundances of condensable species are actually representative of the conditions of hot spots or Jupiter globally.

In this work, we discuss the first observations of the Jupiter's hot spots at 5 μm performed by the Jupiter InfraRed Auroral Mapper (JIRAM) instrument on board the Juno spacecraft in the period of 25–28 August 2016, around the time of the first Juno perijove passage ("PJ1") on 27 August 2016.

2. Data Set

The JIRAM instrument [*Adriani et al.*, 2014] consists primarily of an infrared spectroimager covering the 2–5 μm range with an average spectral sampling of 9 nm/band (average spectral resolution of 15 nm). The spectrometer acquires simultaneously 336 spectra, arranged along a line of spatially contiguous pixels (a "slit"). JIRAM spectra are often complemented by context images acquired integrating the incoming radiance over a broad spectral range centered around 4.8 μm (M-filter imager). The field of view of individual pixels (for the spectrometer as well as for the imager) is about 240 μrad. Since the spectrometer is acquiring one slit at each Juno spacecraft rotation (2 rpm), gaps or overlaps between slits from consecutive rotations may exist, mostly depending upon distance of the spacecraft from target area.

During the first perijove passage of August 2016, JIRAM obtained a fairly complete spatial coverage of the planet, albeit in a variety of emission angles. The region of expected occurrence of the hot spots was observed several times, and this allowed us to select two hot spots for a thorough analysis. For each hot spot, a nominal position of the center at the time of the observation was manually identified as the brightest point observed in the M-filter images. System III [*Archinal et al.*, 2011] is adopted to provide geographic coordinates. Eastward longitudes are considered positive. A summary table of observations is provided in the supporting information.

1. Hot spot #1 was centered at 121.7°E, 8.3°N. Individual JIRAM pixels had a size between 501 and 504 km at the time of the observation. The solar incidence angle ranged between 60° and 70°, while the emission angle ranged between 23° and 35°.
2. Hot spot #2 was centered at −134.4°E, 7.6°N. Individual JIRAM pixels had a size between 234 and 237 km at the time of the observation. The solar incidence angle ranged between 80° and 90°, while emission angles ranged between 14° and 28°.

For each hot spot, we selected the JIRAM (spectrometer) pixels within 5000 km of the nominal position center for the analysis of the atmospheric composition.

In this preliminary investigation we limited our analysis to the spectral range between 4 and 5 μm. Despite its scientific interest, the inclusion of the solar-dominated 2–4 μm range would require the treatment of solar scattering, with significant computational burden and considerable uncertainties on the forward modeling

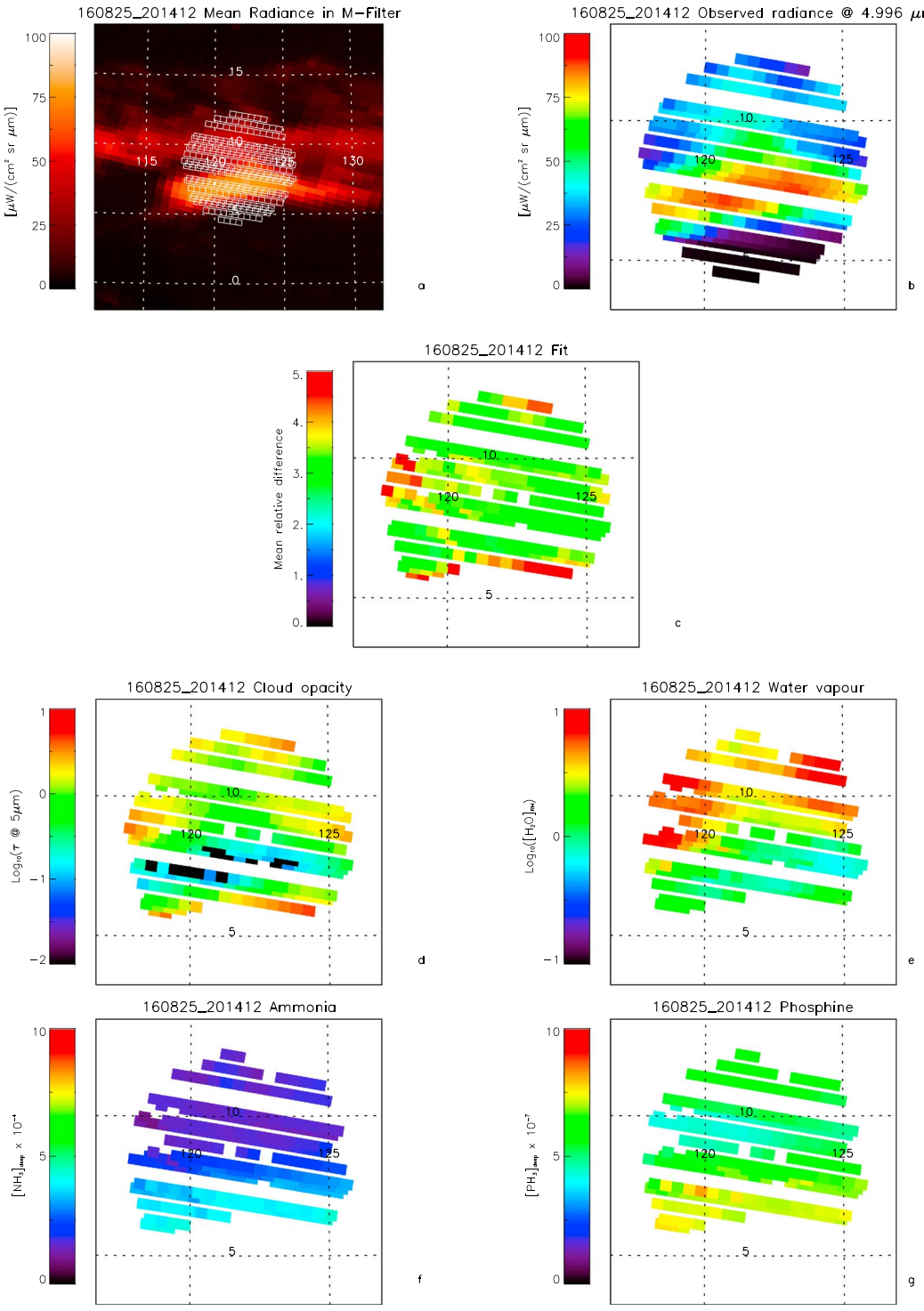

Figure 1. Results for hot spot #1. System III [*Archinal et al.*, 2011] is adopted for geographic coordinates. Eastward longitudes are considered positive. (a) Context image from data of JIRAM imager (M-filter at 5 μm). The white boxes show the locations of individual pixels of JIRAM spectrometer considered in the analysis. Note that absolute radiometric calibration of JIRAM imager is still in progress, and therefore, radiometric values shall be considered preliminary. (b) Corresponding radiances measured at 4.996 μm by the JIRAM spectrometer. (c) Fit quality, quantified as the average relative difference between observed and best fit spectrum in the range of 4.6–5 μm. Only pixels with a fit quality <5% were retained for subsequent analysis. (d) Retrieved cloud opacity (assumed to reside at the 1 bar level) at 4.996 μm. Note the logarithmic scale. Only pixels with $\tau < 2$ were retained for subsequent analysis. (e) Retrieved water vapor relative humidity. Note the logarithmic scale. (f) Retrieved ammonia volume mixing ratio. (g) Retrieved phosphine volume mixing ratio.

errors related to the assumptions of the cloud properties (this is especially true for the upper cloud deck and haze). On the other hand, the "no solar source" approximation is partly justified by our specific focus on these bright areas (assumed to be relatively depleted in clouds), where *Drossart et al.* [1998] reported that scattered solar contribution in the 4–5 μm region should be between 100 and 800 times smaller than the thermal component.

The information content of JIRAM spectra has been discussed extensively in *Grassi et al.* [2010]. In this analysis, we adapted a Bayesian retrieval code previously developed for the study of Visible and Infrared Thermal Imaging Spectrometer-Venus Express data [*Grassi et al.*, 2014]. Free parameters of the spectral fit were (1) the relative humidity of water vapor, (2) the deep (few bars) mixing ratio of ammonia, (3) the mean mixing ratio of phosphine (which contributes to the spectral absorption in this spectral region), and (4) the residual opacity of the 1 bar cloud at 5 μm. Relative retrieval errors on these parameters are estimated to be on the order of 10% and increase to about 20% for ammonia. The performance of the retrieval code has been estimated on the basis of test runs on large sets of simulated observations, and the reported retrieval errors include the effects of forward modeling errors in the radiative transfer. Notably, these errors exceed by at least a factor of 10 the instrumental noise equivalent radiance, as recently estimated in *Adriani et al.* [2016]. This apparently poor performance of the forward modeling must seen in the context of a very high JIRAM signal-to-noise ratio, exceeding 500 in the hot spots observation. Under these conditions, it is convenient to quantify the fit quality (quality parameter) as the average relative difference between the best fit and the observed spectrum in a given spectral range (4.6–5 μm in our case) rather than rely on the usual χ^2 value. Two examples of spectral fits of JIRAM data from the two hot spots are presented in the supporting information.

3. Results

Figures 1 and 2 summarize the results of the retrievals for the two hot spots.

We will discuss separately the two areas. For the sake of brevity, the standard radiance unit of 1 μW/(cm^2 sr μm) as measured at 4.996 μm is hereafter referred to as 1 RU. The retrieved quantities of Figures 1d–1g and 2d–2g are shown only when the fit quality parameter is smaller than 5%. The retrieved values of the gas parameters (Figures 1e–1g and 2e–2g) are shown only if the corresponding retrieved cloud opacity at 5 μm is less than 2. Such a threshold on opacity is required because of the rapid increase in retrieval errors on the parameters describing the gas distribution in the deep (approximately several bars) troposphere. They do so because the relative contribution from these areas to the observed total radiation becomes small due to absorption of radiation by clouds.

3.1. Hot Spot #1

Figure 1 presents the results for hot spot #1. Its structure appears elongated along the longitude, with an approximate size of 10^4 km by 5×10^3 km. The appearance of the hot spot is not uniform: at least three distinct radiance maxima can be identified in the brighter area. While the southern rim of the hot spot is relatively sharp (rising from 5 RU to 75 RU in about 1500 km), the decrease of the radiance toward the north is much smoother and the boundary of the hot spot is blurred in the average brightness of the North Equatorial Belt. Taking into account the different reference wavelength and spectral resolutions, the maximum signal observed in hot spot #1 is compatible with the values reported by *Roos-Serote et al.* [1998] and *Nixon et al.* [2001] for their brighter study cases from NIMS data. The fit quality parameter is not uniform, being considerably better in the regions of high signal. In the southernmost observations over cloudier areas, it exceeds the threshold value of 5%, and hence, the corresponding pixels are not shown on the maps.

The brightest of several pixels shows opacities lower than 0.1; therefore, they are considerably more transparent than the ones documented by the Galileo Entry Probe Net Flux Radiometer on its C channel [*Sromovsky et al.*, 1998] or the NIMS real-time spectra discussed by *Irwin et al.* [1998]. Not surprisingly, the retrieved opacity (Figure 1b) shows a high degree of anticorrelation with measured radiance (Figure 1d). The range of values of opacity is, however, consistent with the highly nonuniform nature of the hot spot center. A similar scenario has been discussed in the analysis of Cassini Imaging Science Subsystem (ISS) data by *Choi et al.* [2013], where a number of transient phenomena (high-altitude fast clouds and putative deepwater clouds) correlate with inhomogeneities at hot spot centers in the visible spectral range. Future analysis of JIRAM

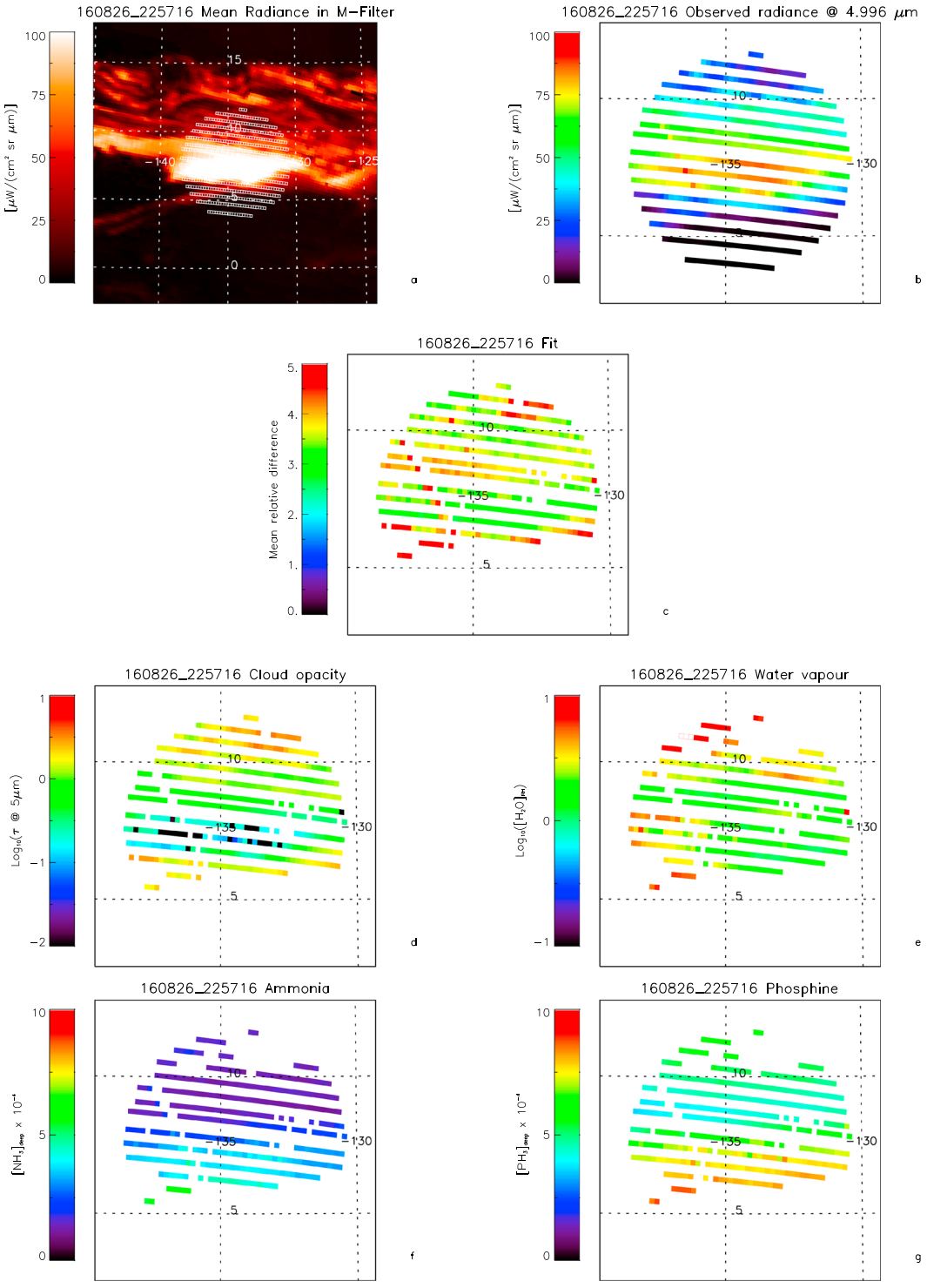

Figure 2. As in Figure 1 but for hot spot #2.

data including the solar spectral range is expected to characterize cloud altitudes and thus relate the local opacity enhancements reported here to the phenomena observed in the ISS data.

The water relative humidity is below 10% for the entire region where the gas retrievals were performed. *Irwin et al.* [1998], *Roos-Serote et al.* [1998], and *Nixon et al.* [2001] found that bright areas usually appear drier than

the surroundings. However, we found that locations where the relative humidity is lower than 1% (e.g., 7.5°N, 125°E) do not correspond exactly to the brightest regions, but they seem preferentially located on their east side. It should also be noted that our retrieved relative humidity values usually appear a factor of 5 to 8 higher than those found by *Roos-Serote et al.* [1998] for similar opacity conditions and similarly higher than the values presented by *Nixon et al.* [2001]. This discrepancy with respect to NIMS estimates is not explained by the better spectral resolution of JIRAM or by the most recent spectral line databases considered in our analysis. More likely, the cause lies in the inclusion by both *Roos-Serote et al.* [1998] and *Nixon et al.* [2001] of a water deep cloud (with a top located around 5 bars) in their atmospheric models. We find that such a feature can induce variations up to a factor of 3 on retrieved content of water (with amplitudes strongly dependent on assumed cloud properties) without substantial variations in fit quality. Albeit the high-spectral resolution measurements discussed by *Giles et al.* [2016] suggest that a water deep cloud can be present at most latitudes on Jupiter, it would in any case tend to vanish at the typical hot spot latitudes. The large-scale latitudinal trends for water vapor presented by *Giles et al.* [2015] in their Figure 13 is also only marginally consistent ($1.2 \pm 0.5\%$) with our retrievals in the regions surrounding the brightest part of the hot spot.

In most of the northern part of the studied region the retrieved value of the ammonia mixing ratio is approximately 200 ppmv, slowly increasing to ~400 ppmv at the southern boundary of the hot spot. The ammonia abundance appears to be largely correlated with latitude rather than with absolute radiance and increases steadily toward the equator. Notably, the Juno Microwave Radiometer (MWR) also observed a sharp increase of ammonia moving southward from typical hot spot latitudes [*Li et al.*, 2017], though the track of MWR did not overpass any of our observed features during the PJ1 passage. A comparison against the in situ measurements by the Galileo Probe mass spectrometer (GPMS [*Atreya et al.*, 1999; *Wong et al.*, 2004]) or the values derived from probe's radio attenuation data (RA) [*Folkner et al.*, 1998] can be properly performed only taking into account the actual pressure range probed by the JIRAM data. *Grassi et al.* [2010] presented the partial derivatives of JIRAM radiances with respect to ammonia mixing ratio (Figures 2b and 2c): these functions turned out to be relatively broad, with substantial contributions between 4 and 6.5 bars. The 5 bar level can be roughly assumed as the barycenter of JIRAM sensitivity. On the other hand, the Galileo Probe experiments measured NH_3 as a function of atmospheric pressure. Under the simplest conditions (namely, absence of large-scale descending motions) one would expect that ammonia reaches its "bulk" mixing ratio (representative of its abundance in the planet as a whole) just below its condensation level. The Galileo Probe data showed, however, that NH_3 was greatly subsolar well below the expected NH_3 cloud base (approximately 0.7 bar, for 3 times solar N/H) but reached more than twice the solar value at 5 bars (~330 ± 130 ppmv at 5 bars [*Folkner et al.*, 1998]) and a well-mixed value of 700 ± 100 ppmv by RA and 572 ± 218 ppmv by GPMS only at 8 bars, much deeper than the pressure levels probed by JIRAM. The JIRAM and GEP values at the 5 bar level are therefore consistent within the error bars in the entire hot spot #1, with the best agreement being achieved at the southern rim, in a position corresponding to the entry site of the Galileo Probe.

The phosphine volume mixing ratio varies between 4×10^{-7} and 8×10^{-7}. Its abundance increases from north moving toward the equator, but with a local minimum (9°N, 120°E) just north of the brightest region of the hot spot. Overall, the phosphine values are consistent with the global latitudinal trends inferred from VIMS-Cassini data [*Giles et al.*, 2015] and ground-based observations [*Giles et al.*, 2016]. The phosphine maps presented by *Fletcher et al.* [2009] also suggest an increase of the mixing ratio from latitude 10°N toward the equator. Note, however, that the spectral range used in that work (8–12 μm) probes pressures below 1 bar, lower (hence higher in altitude) than the peaks of JIRAM weighting functions, limiting therefore the validity of a comparison of absolute values.

In the context of JIRAM's data collected during PJ1, hot spot #1 observations were acquired at a relatively large distance and, in a few cases, the spectrometer swaths overlap, allowing an assessment of the robustness of the retrieval scheme. In general, overlapped pixels show highly correlated retrieved values of the atmospheric parameters (differences are within 10% and consistent with systematic spatial gradients), corroborating our confidence in the overall performance of the code.

3.2. Hot Spot #2

Figure 2 presents the results for hot spot #2. The structure appears brighter than hot spot #1, consistent with the lower emission angle of this observation (which implies a shorter optical path of the line of sight through

the residual cloud layer). The size and overall morphology of the structure appear similar to its previously described counterpart hot spot #1. Namely, the opacity of the atmosphere (still strongly anticorrelated with measured radiance) appears to have a complex pattern inside the brighter area, with a few local distinct minima. Similarly, the southern boundary appears sharp, while the hot spot tends to disappear more gradually toward north. The range of the observed opacities remains essentially the same in the two regions.

However, some differences can be seen in the gas abundance maps. The water vapor depletion region is more extended toward the north. On the west side of the studied region (138°W, 7.5°N) a number of sites with relatively high relative humidity (>3%) in the transparent regions are visible. Moreover, hot spot #2 does not show relative humidity below 1%. Drier areas (but still above 1% relative humidity) are again located immediately east of the brightest pixels.

The ammonia abundances in hot spot #2 are consistent with those in hot spot #1, but at the southern border of the observed area a few cases of mixing ratios close to 600 ppmv have been observed. Again, this suggests that the values of ammonia are poorly correlated with the overall brightness and are instead driven by latitudinal trends. The more southerly regions of hot spot #2 actually appear richer in ammonia than hot spot # 1, with the difference being larger than the estimated retrieval uncertainty of 20%. The intrinsic case-to-case variability of these structures represents an important point to consider when comparing JIRAM and Galileo Probe estimates. We also observe a tendency of ammonia to decrease toward the eastern part of the hot spot approximately at the latitude of the feature's center.

Similar to what is observed in hot spot #1, the phosphine content tends to increase toward the south, with a latitudinal minimum just north of the brightest area. The range of absolute values of mixing ratios for this molecule is similar in the two areas.

4. Discussion

The JIRAM observations of the two hot spots can be summarized as follows:

1. In the hot spots observed by JIRAM, ammonia increases toward their center, but this trend is most likely related to a general southward increase of ammonia than to a correlation with the brightness itself (Figure 2f). The ammonia mixing ratios retrieved from JIRAM data are consistent with the range of values (~200–450 ppmv, including error bars) reported by the Galileo Probe for the levels of JIRAM peak sensitivity centered at approximately 5 bars. Our analysis consistently points toward values lower than 600 ppmv, a value reached only in the southernmost boundaries of hot spot #2. While this extreme value is still compatible with the deep ammonia values measured by the GPMS experiment *at pressures greater than 8 bars* in another hot spot, it appears much larger than the well-mixed value of 350 ppmv obtained by Juno MWR. While the JIRAM values are generally consistent with those derived near the 5 bar level by MWR [*Orton et al.*, 2017] from co-located measurements, we stress that MWR has not yet sampled a hot spot directly. A possible scenario therefore seems to be that hot spots are sites of anomalous ammonia enhancement, at least in their southern areas.
2. Hot spots show complex patterns in the distribution for the other two observed gases, PH_3 and H_2O. The water vapor content is lower in the brighter regions (as defined by $\tau < 0.3$) than in the surrounding moderate opacity areas. However, drier pixels do not exactly correspond to the brighter ones. Instead, they consistently appear at the immediate east side of the bright regions (compare Figures 2d and 2e). For phosphine, again, the overall impression is that its abundance tends to increase toward the south, but a local, moderate decrease is associated with areas just north of more transparent ones (namely, the latitudinal minimum at 8°N in Figure 2g).

While preliminary, these results confirm that large parts of the hot spots are regions of downward motion, related to general dry conditions of the atmosphere. This scheme is also consistent with smaller amounts of phosphine—considered to be a tracer of upward motions—toward the hot spot centers [*Fletcher et al.*, 2009]. The consistent patterns of water vapor (which shows a minimum eastward of the areas of maximum brightness) and phosphine (which shows a minimum northward of the areas of maximum brightness) will be useful in defining an updated dynamical model for these structures. Note, however, that our gas mixing ratio maps also suggest the occurrence of *upward* motions of the atmosphere at the southern rims of the hot

spots: the rise of phosphine and ammonia toward the equator (before the clouds become too thick for JIRAM to provide meaningful measurements) is particularly significant. While MWR provides a clear hint of the rise of ammonia from very deep atmosphere (down to 200 bars) at equatorial latitudes on global scale, both JIRAM and—retrospectively—Galileo Probe data suggest further local enhancements of ammonia related to specific conditions within the hot spots.

The general morphology of the hot spots discussed here (Figures 1a and 2a) is close to that of similar spots studied in visible images by Voyager [see *Hueso and Sánchez-Lavega*, 1998, Figure 1] and Galileo [see *Vasavada et al.*, 1998, Figure 9], and one stage of the evolution of hot spots studied by Cassini [see *Choi et al.*, 2013, Figures 4, 5a, 6a–6c, and7a]. The wind fields derived from the Galileo [*Vasavada et al.*, 1998] and Cassini [*Choi et al.*, 2013] are consistent in their assessment of typical flow patterns. The spots at this stage are bounded to the north and south by westward mean zonal winds, with cyclonic motion to their west and anticyclonic motion to their east and southeast. The latter define their eastern and western boundaries, as well as a faint southwest trailing extension, such as seen in Figure 2a. Those studies did not describe wind motions within hot spots, so there are no direct comparisons with our results except to the extent that they define the coincident visible and infrared boundaries of the spots, as noted by *Orton et al.* [2017], that are highly correlated with our derived cloud-opacity fields (Figures 1d and 2d).

Because of the importance of understanding the unexpected Galileo Probe results, several models have been constructed that used entrained, dry, downwelling motions to explain the desiccated composition and absence of thick clouds. *Hueso et al.* [1999] explained this and the spacing of hot spots in longitude by invoking a vertical Rossby wave, consistent with the suggestion by *Ortiz et al.* [1998], who addressed the measured longitudinal structure and lifetime of hot spots. *Showman and Dowling* [2000] attempted to simulate coupled vertical and horizontal winds with a sophisticated numerical model. They emphasized that a strong vertical wind shear develops near the southern edge of their hot spot models, even when it is much weaker elsewhere, because it is associated with a stagnant region inside an anticyclonic gyre south of hot spots that overlies faster, deep flow. Qualitatively, this implies generally stronger desiccation toward the southern edge of the hot spot. However, their model did not achieve the desiccation detected by the Galileo probe, and we observe increased ammonia abundance from the center to the southern edge and generally increased phosphine abundances.

Friedson [2005] expanded on their work by modeling the wave in terms of an amplitude-saturated, equatorially trapped Rossby wave that required pressure variations on constant potential-temperature surfaces to reach ~20 bars, sufficient to match the Probe results. However, his expectations of a rise of volatile abundances at the eastern side of hot spots [Friedson, 2005, Figures 9 and 10] are also not supported by our observations, where water (Figure 1e) and ammonia (Figure 2f) appear to diminish on the east portion of hot spots. These observations can be possibly reconciled with the model if we assume that a substantial fraction of the actual eastern area of the hot spot is being masked by relatively high clouds on the eastern side. This scenario is consistent with the observations of *Hueso and Sánchez-Lavega*, 1998 of "narrow frontal lines of clouds" (their Figure 1c), as well as with the discussion of *Choi et al.* [2013] regarding their Figure 9, but it can be confirmed only when a complete analysis of cloud heights based on the analysis of JIRAM spectra in the solar range is accomplished. We underscore *Friedson*'s [2005] call for greater sophistication in models, coupled with (i) the need to understand the complicated deeper-atmospheric structure evident in MWR results for ammonia (e.g., Figure 2 of *Orton et al.* [2017] and MWR articles in this issue) and (ii) the importance of MWR measurements of a 5 μm hot spot.

5. Conclusions

JIRAM spectra acquired for two bright hot spots during the first Juno perijove passage have been analyzed in the 5 μm transparency window. Our results imply a major role of large-scale latitudinal variations in the abundances of trace gases, with water vapor and phosphine playing an important role as proxies for local hot spot vertical dynamics. The retrieved content of ammonia is also possibly indicative of vertical motions occurring within the hot spots.

The results reported in this paper are the first obtained from JIRAM observations and therefore should be regarded as preliminary. The comparison between the ammonia abundances estimated in this work with

those measured by the GEP and the Juno MWR will need to be further explored through the additional spectra from PJ1 that have still to be analyzed. Inclusion of shorter wavelength, solar-dominated spectral ranges in the future analyses will provide insights on the cloud structure and allow for testing the preliminary conclusions on vertical dynamics drawn here.

Acknowledgments
This work was supported by the Italian Space Agency through ASI-INAF contract I/010/10/0 and 2014-050-R.0. J.I.L. and S.K.A. acknowledge support from NASA through the Juno Project. G.S.O. acknowledges support from NASA through funds that were distributed to the Jet Propulsion Laboratory, California Institute of Technology. The retrieval code is based on the ARS software, developed by Nikolay Ignatiev, Space Research Institute of the Russian Academy of Sciences. Tiziano Maestri (University of Bologna) is acknowledged for his software tools and extensive discussion. Development of the retrieval code greatly benefited of discussions with P. Irwin, L. Fletcher, R. Giles, T. Fouchet, P. Drossart, M. Roos-Serote, and L. Kedziora-Chudczer. The JIRAM instrument has been developed by Leonardo at the Officine Galileo, Campi Bisenzio site. The JIRAM instrument was conceived and brought to reality by our late collaborator and institute director Angioletta Coradini (1946–2011).

References

Adriani, A., et al. (2014), JIRAM, the Jovian Infrared Auroral Mapper, *Space Sci. Rev.*, 1–54, doi:10.1007/s11214-014-0094-y.
Adriani, A., et al. (2016), Juno's Earth flyby: The Jovian infrared auroral mapper preliminary results, *Astrophys. Space Sci.*, *361*(8), 272.
Archinal, B. A., et al. (2011), Report of the IAU working group on cartographic coordinates and rotational elements: 2009, *Celest. Mech. Dyn. Astron.*, *109*, 101–135, doi:10.1007/s10569-010-9320-4.
Arregi, J., et al. (2006), Phase dispersion relation of the 5-micron hot spot wave from a long-term study of Jupiter in the visible, *J. Geophys. Res.*, *111*, E09010, doi:10.1029/2005JE002653.
Atreya, S. K., et al. (1999), Comparison of the atmospheres of Jupiter and Saturn: Deep atmospheric composition, cloud structure, vertical mixing, and origin, *Planet. Space Sci.*, *47*, 1243–62, doi:10.1016/S0032-0633(99)00047-1.
Carlson, B. E., et al. (1993), Tropospheric gas composition and cloud structure of the Jovian north equatorial belt, *J. Geophys. Res.*, *98*(E3), 5251–5290, doi:10.1029/92JE02737.
Choi, D., et al. (2013), Meteorology of Jupiter's equatorial hot spot and plumes from Cassini, *Icarus*, *223*, 832–843, doi:10.1016/j.icarus.2013.02.001.
Drossart, P., et al. (1998), The solar reflected component in Jupiter's 5-μm spectra from NIMS/Galileo observations, *J. Geophys. Res.*, *103*(E10), 23,043–23,049, doi:10.1029/98JE01899.
Fletcher, L. N., et al. (2009), Phosphine on Jupiter and Saturn from Cassini/CIRS, *Icarus*, *202*, 543–564, doi:10.1016/j.icarus.2009.03.023.
Fletcher, L. N., et al. (2016), Mid-infrared mapping of Jupiter's temperatures, aerosol opacity and chemical distributions with IRTF/TEXES, *Icarus*, *278*, 128–161, doi:10.1016/j.icarus.2016.06.008.
Folkner, W. M., et al. (1998), Ammonia abundance in Jupiter's atmosphere derived from attenuation of the Galileo probe's radio signal, *J. Geophys. Res.*, *103*, 22,847–2,856, doi:10.1029/98JE01635.
Friedson, A. J. (2005), Water, ammonia, and H_2S mixing ratios in Jupiter's five-micron hot spots: A dynamical model, *Icarus*, *177*, 1–17, doi:10.1016/j.icarus.2005.03.004.
Giles, R. S., et al. (2015), Cloud structure and composition of Jupiter's troposphere from 5-micron Cassini VIMS spectroscopy, *Icarus*, *257*, 457–470, doi:10.1016/j.icarus.2015.05.030.
Giles, R. S., et al. (2016), Latitudinal variability in Jupiter's tropospheric disequilibrium species: GeH4, AsH3 and PH3, *Icarus*, doi:10.1016/j.icarus.2016.10.023, in press.
Grassi, D., et al. (2010), Jupiter's hot spots: Quantitative assessment of the retrieval capabilities of future IR spectro-imagers, *Planet. Space Sci.*, *58*, 1265–1278, doi:10.1016/j.pss.2010.05.003.
Grassi, D., et al. (2014), The Venus nighttime atmosphere as observed by the VIRTIS-M instrument. Average fields from the complete infrared data set, *J. Geophys. Res. Planets*, *119*, 837–849, doi:10.1002/2013JE004586.
Hueso, R., and A. Sánchez-Lavega (1998), Motions in hot spot-plume regions using Voyager images, *Icarus*, *136*, 353–357, doi:10.1006/icar.1998.6018.
Hueso, R., et al. (1999), A theoretical study of parcel stability and cloud distribution in a Jovian hot spot, *Planet. Space Sci.*, *47*, 1263–1275, doi:10.1016/S0032-0633(99)00049-5.
Irwin, P. G. J., et al. (1998), Cloud structure and atmospheric composition of Jupiter retrieved from Galileo near-infrared mapping spectrometer real-time spectra, *J. Geophys. Res.*, *103*(E10), 23,001–23,021, doi:10.1029/98JE00948.
Irwin, P. G. J., et al. (2001), The origin of belt/zone contrasts in the atmosphere of Jupiter and their correlation with 5-μm opacity, *Icarus*, *149*, 397–415, doi:10.1006/icar.2000.6542.
Li, C., et al. (2017), Jupiter's global ammonia distribution from inversion of Juno Microwave Radiometer observations, *Geophys. Res. Lett.*, doi:10.1002/2017GL073159, in press.
Niemann, H. B., et al. (1998), The composition of the Jovian atmosphere as determined by the Galileo probe mass spectrometer, *J. Geophys. Res.*, *103*(E10), 22,831–22,845, doi:10.1029/98JE01050.
Nixon, C. A., et al. (2001), Atmospheric composition and cloud structure in Jovian 5-μm hotspots from analysis of Galileo NIMS measurements, *Icarus*, *150*, 48–68, doi:10.1006/icar.2000.6561.
Ortiz, J. L., et al. (1998), Evolution and persistence of 5-μm hot spots at the Galileo probe entry latitude, *J. Geophys. Res.*, *103*, 23,051–23,069, doi:10.1029/98JE00696.
Orton, G. S., et al. (1998), Characteristics of the Galileo Probe entry site from Earth-based remote sensing observations, *J. Geophys. Res.*, *103*, 22,791–22,814, doi:10.1029/98JE02380.
Orton, G. S., et al. (2017), Multiple-wavelength sensing of Jupiter from the Juno mission and contemporaneous Earth-based observations, *Geophys. Res. Lett.*, *44*, doi:10.1002/2017GL073019, in press.
Rogers, J. H. (1995), *The Giant Planet Jupiter*, Univ. Press, Cambridge.
Roos-Serote, M., et al. (1998), Analysis of Jupiter north equatorial belt hot spots in the 4–5 μm range from Galileo/near-infrared mapping spectrometer observations: Measurements of cloud opacity, water, and ammonia, *J. Geophys. Res.*, *103*(E10), 23,023–23,041, doi:10.1029/98JE01049.
Roos-Serote, M., et al. (1999), Constraints on the tropospheric cloud structure of Jupiter from spectroscopy in the 5-μm region: A comparison between Voyager/IRIS, Galileo/NIMS, and ISO/SWS Spectra, *Icarus*, *137*, 315–340, doi:10.1006/icar.1998.6043.
Sromovsky, L. A., et al. (1998), Galileo Probe measurements of thermal and solar radiation fluxes in the Jovian atmosphere, *J. Geophys. Res.*, *103*, 22,929–22,978, doi:10.1029/98JE01048.
Showman, A. P., and T. E. Dowling (2000), Nonlinear simulations of Jupiter's 5-micron hot spots, *Science*, *289*, 1737–1740, doi:10.1126/science.289.5485.1737.
Terrile, R. J., and J. A. Westphal (1977), The vertical cloud structure of Jupiter from 5 micron measurements, *Icarus*, *30*, 274–281, doi:10.1016/0019-1035(77)90159-2.

Vasavada, A. R., et al. (1998), Galileo imaging of Jupiter's atmosphere: The Great Red Spot, equatorial region and white ovals, *Icarus*, *135*, 265–275, doi:10.1006/icar.1998.5984.

Wong, M. H., et al. (2004), Updated Galileo probe mass spectrometer measurements of carbon, oxygen, nitrogen, and sulfur on Jupiter, *Icarus*, *171*(2004), 153–170, doi:10.1016/j.icarus.2004.04.010.